Scripta Materialia 219 (2022) 114857

Contents lists available at ScienceDirect

Scripta Materialia

journal homepage: www.journals.elsevier.com/scripta-materialia

Nucleation and growth kinetics of $ZnAl_2O_4$ spinel in crystalline ZnO – amorphous Al_2O_3 bilayers prepared by atomic layer deposition

Gabriella Jáger [a,b], János J. Tomán [a,*], Laura Juhász [a], Gergő Vecsei [a,b], Zoltán Erdélyi [a], Csaba Cserháti [a]

[a] Department of Solid State Physics, Faculty of Science and Technology, University of Debrecen, PO Box 400., Debrecen H-4002, Hungary
[b] Doctoral School of Physics, University of Debrecen, Debrecen, Hungary

ARTICLE INFO

Keywords:
Ceramic thin films
Binary oxides
Nucleation of phase transformations
Phase transformation kinetics
Spinel

ABSTRACT

Applying scanning electron microscopy in transmission mode and grazing incidence X-ray diffraction, we investigated the spinel-forming solid-state reaction between crystalline ZnO and amorphous Al_2O_3 layers prepared by atomic layer deposition. We observed two-stage phase growth of the crystalline $ZnAl_2O_4$ product layer. During the first stage, flat, pancake-like islands are formed in the nucleation process and these nuclei grow laterally without much increment in thickness. After these islands grow together to form a continuous layer, planar growth is happening in the second stage. We show that the solid-state reaction is governed by grain boundary and interface diffusion instead of interface reaction control observed between crystalline parent phases.

Spinel type materials have a general formula of AB_2O_4, where both A and B are metals, and A is divalent, while B is trivalent. This group of materials have attracted considerable interest recently due to their excellent optical, electronic and catalytic properties [1]. Zinc-aluminate ($ZnAl_2O_4$ or gahnite) spinel is receiving special attention due to its especially useful optical and catalytic properties. The possible future applications span a wide variety of fields. $ZnAl_2O_4$ can be used as a catalyst in the removal of air polluting agents; e.g. reduction of NO_x by hydrocarbons [2]. It is a promising photocatalyst to degrade toxic aromatic compounds like toluene [3] and it can also catalyse CO hydrogenation to methanol/dimethyl ether [4]. Furthermore, it might be applicable as a sensor thanks to the fact that its luminescence spectrum strongly depends on its thermal history [5]. With doping, the colour of its photoluminescence is finely controllable and can be used as a phosphor [6]. Its nonlinear optical properties make it a potential optical limiter material [7]. Zinc-aluminate can also be very interesting for the solar energy industry, as it has recently been shown to be suitable as an antireflective coating material to improve the power conversion efficiency of silicon solar cells [8].

Other than its great material properties, the many different available methods of producing $ZnAl_2O_4$ makes it an industrially applicable material. Production flexibility is a key for the industry to enable the optimization of fabrication costs. Zinc-aluminate can be produced e.g. via sol-gel method [9], hydrothermal synthesis [10], solid-gas reaction [11], molten salts [12] and solid-state reaction. In our work we will focus on the latter one, namely the solid-state reaction between ZnO and Al_2O_3. Not many studies have investigated the reaction kinetics in this binary system. In [13] the authors determined the growth kinetics of the product phase between two crystalline layers of the parent phases. The reaction clearly showed a linear phase growth in time, indicating an interface controlled reaction.

The formation of zinc-aluminate spinel in the solid-state reaction of ZnO and Al_2O_3 started to attract considerable attention when, with the right initial setup, it produced hollow $ZnAl_2O_4$ or laminated composite nanotubes [14–22]. For this behaviour to take place, the initial samples were multilayered cylindrical structures with crystalline ZnO and amorphous Al_2O_3 layers, usually prepared by atomic layer deposition (ALD). ALD is a great tool to uniformly coat cylindrical templates, let them be nanowires [19] or cylindrical holes [22].

A great starting template to produce the initial multilayered, cylindrical samples are polymer nanowires. These can be easily removed by heating the system in air at an elevated temperature [19,23]. At first, the samples were heated to 230°C with 10°C/min rate, then the heating rate was lowered to 2°C/min to avoid damaging the nanotube structure, when the most intense gas release and combustion occurred. The annealing was finished at 550°C by quenching the sample [23].

* Corresponding author.
E-mail address: janos.toman@science.unideb.hu (J.J. Tomán).

https://doi.org/10.1016/j.scriptamat.2022.114857
Received 14 February 2022; Received in revised form 12 May 2022; Accepted 6 June 2022
Available online 22 June 2022

To investigate the details of spinel formation in the reaction between ALD-deposited crystalline ZnO and amorphous Al_2O_3 layers, we prepared bilayered, planar thin film samples in a Beneq TFS-200-186 reactor by low-temperature (100°C) thermal ALD on Si(1 1 1) substrates with their native oxide layers. The Al_2O_3 layer was prepared using trimethylaluminium (TMA) and water (H_2O) as precursors. The ZnO layer was prepared from diethylzinc (DEZ) and water (H_2O) as precursors.[1] The average thicknesses of the grown layers were determined by evaluating transmission mode scanning electron microscope (TSEM) images (see Fig. 1a). For alumina it was 88.4 nm, while the average thickness of the ZnO layer was 163.1 nm.

With these deposition conditions, ZnO is growing in the wurtzite crystal structure. Preferential growth have been observed previously, and the preferred crystal orientations depend strongly on the deposition temperature, substrate material and orientation [24–30]. Aluminium-oxide thin films prepared by ALD are known to be amorphous and the O/Al ratio in them is the stoichiometric 1.5 [31,32], which we also confirmed by energy dispersive X-ray spectroscopy (EDS) in a transmission electron microscope.

To avoid the reaction between ZnO and the native oxide of the Si substrate, we have purposefully chosen the following layer order: Si/Al_2O_3/ZnO. The initial interface sharpness between the two investigated layers is determined by the layer uniformity of the bottom layer, so this layer structure has the added benefit that since the amorphous alumina layer produced by ALD is extremely flat, the initial interface was extremely sharp, too.

Lamellae that can be examined in transmission mode were prepared from the samples using a focused ion beam scanning electron microscope (FIB-SEM) and images were taken in transmission mode in the same scanning electron microscope.

In the image of the as-deposited sample (Fig. 1a), one can observe a very flat and sharp initial interface between the amorphous Al_2O_3 and the crystalline ZnO.

To make our results in the planar samples comparable to the ones produced with initial polymer cores, which then are removed by burning out, we also performed the same pre-treatment step (to 230°C with 10°C/min, to 550°C with 2°C/min, then quench) in air atmosphere using a tube furnace. Of course, in our case no combustion happens as there is no polymer in the system, but our motivation was to investigate if this pre-treatment step is sufficient to initiate the solid-state reaction between the two layers.

After this first heat treatment, the sample shows no structural change (Fig. 1b). We performed subsequent, isothermal heat treatments on the same sample, in the same furnace, in air atmosphere at 700 °C. Both the introduction and the removal of the sample happened at this temperature, so the heating and cooling times are negligible compared to the actual heat treatment times. Based on previously published results, at this temperature the formation of a reaction product was expected [14,17,19], which was confirmed by TSEM images (see Fig. 1c–f).

Grazing incidence X-ray diffractograms (GIXRD) were collected under Cu-Kα radiation using an X-ray diffractometer (see Fig. 2). Incident angle was $\omega = 1.3^{\circ}$, which corresponds to at least 800 nm penetration depth in ZnO [33,34]. No reaction product was visible after the pre-treatment (to 230°C with 10°C/min, to 550°C with 2°C/min, then quench). The only peaks in the diffractogram are from the crystalline ZnO as the ALD-deposited Al_2O_3 layer was amorphous. The GIXRD measurements, performed on the annealed samples, confirmed that the reaction product visible on the TSEM images is indeed crystalline $ZnAl_2O_4$. Note that no Al_2O_3 peaks appear even after a very long heat treatment as the crystallization of ALD-prepared amorphous alumina does not start below 800°C [35].

In Fig. 2, the peak at 34.45° corresponding to ZnO (0 0 2) planes shows a significant decrease in intensity. The change in the relative intensities of XRD peaks during heat treatments of ZnO thin films by atomic layer deposition have been observed before [24,27]. Generally, the crystal orientation that was preferred during deposition (in this case (1 0 0)) will gain higher dominance during the additional annealing. One must note, that due to the many overlapping XRD peaks between $ZnAl_2O_4$ and ZnO, it is hard to draw a quantitative conclusion about the relative weights of the ZnO peaks, but the goal of these measurements was to identify the reaction product.

After 15 min at 700°C, islands of the new phase are clearly identifiable in the TSEM images (see Fig. 1c). The new phase is very clearly located on the amorphous alumina side of the initial interface, indicating that the oxygen and zinc ions of ZnO are the only diffusing species. This is in clear agreement with the experimental findings in nanowires, where amorphous alumina was used as well [14–17,19,22,37]. We must note though, that this is very different from the findings in planar systems with crystalline Al_2O_3 and ZnO layers, where the reaction product grows in the directions of both parent phases, indicating that in those cases both species diffuse into each other [13,38].

Apart from the location of the formed phase, another strong indicator of the asymmetric diffusion in the system is the appearance of the Kirkendall voids between the product phase islands and the initial ZnO phase (see Fig. 1c).

The Kirkendall effect or Kirkendall shift occurs due to the difference in diffusivities of the components moving in opposite directions and the resulting vacancy flux. These vacancies can annihilate on dislocation kinks and generate a lattice shift which we know as Kirkendall shift. Another way for these vacancies to annihilate is forming voids, these are the Frenkel voids, but most often named as Kirkendall voids in the literature. These two processes are competing with each-other. If one suppresses void formation by an external pressure, the magnitude of the Kirkendall shift will increase [39,40].

Interestingly, these voids do not slow down the reaction. The reason for this is that material transport continues on the walls of voids with surface diffusion, which has a much lower activation energy [15–17,41].

Increasing the annealing time to 30 and 60 min results in the growth of the previously formed islands. But interestingly, the growth happens almost exclusively in lateral direction, parallel to the initial interface and only to a much lesser extent perpendicularly to that (Fig. 1d).

While this “pancake” type of phase nucleation is not unknown to materials science, according to our knowledge this is the first time it was observed in a solid-state reaction between two oxide layers. It was first theorized and predicted by Coffey et al. in 1989 from detailed analysis of differential scanning calorimetric data [42]. In those measurements two peaks can be observed during the solid-state reaction, indicating a two-stage phase formation. The first peak belongs to the nucleation and lateral growth of the product phase nuclei, while the second peak indicates the normal, planar growth of the continuous reaction layer. Similar behaviour has been found in multiple metal-metal and metal-silicon reactions, from which Co-Si and Ni-Si are the most remarkable ones [43–52].

Detailed analysis of the first, lateral growth stage was first attempted by Klinger et al. [53]. Later a more complete picture was drawn in Gusak et al. [39], Lucenko and Gusak [54], Gusak et al. [55], Pasichnyy and Gusak [56]. For an “almost lateral” growth of the initially formed nuclei, the authors had to take a few assumptions. First, bulk diffusion in every phase was completely frozen, meaning that diffusion of the species could happen only along the interphase boundaries of the initial phases and the product phase. At the same interphase boundaries solid-state reaction takes place. As a result of these assumptions, the growth of a product phase island comes to a quasi-stationary state when its maximum thickness reaches an asymptotic value, but its lateral size increases linearly with time.

At the end of the first stage, the lateral growth is naturally terminated by the coalescence of the product islands to a continuous layer. The second stage of phase growth is the planar growth of the reaction layer.

[1] Process parameters and further experimental details can be found in the Supplementary Materials.

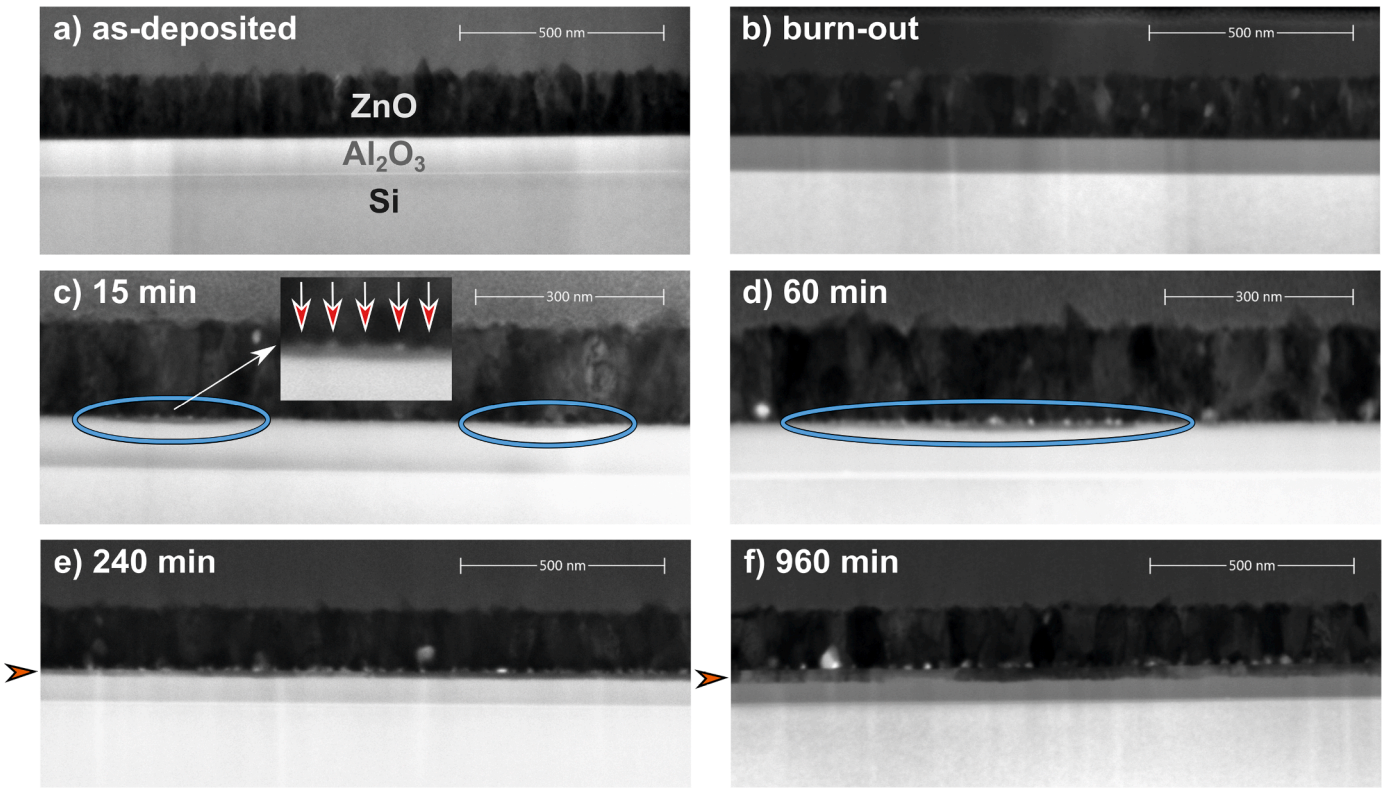

Fig. 1. Transmission mode scanning electron microscopy (TSEM) images of lamellae prepared by focused ion beam from samples after different heat treatments. (a) As-deposited sample with a very sharp interface. (b) After the pre-treatment step (to 230°C with 10°C/min, to 550°C with 2°C/min, then quench), the interface is still sharp and flat. (c) Subsequently annealing the system for 15 min at 700°C results in the formation of flat islands of the reaction product on the Al_2O_3 side of the initial interface (marked by the ellipses). The magnified detail with the arrows shows the tiny Kirkendall voids appearing on the initial interface where the reaction product forms. (d) Annealing the system for 60 min at 700°C results in islands that increased in lateral size significantly, but much less in thickness. The significant increase in the size of the Kirkendall voids is also evident. (e) Annealing the system for 240 min at 700°C, the reaction product forms a continuous layer (marked by the arrow) with Kirkendall voids scattered everywhere at the initial interface. (f) With the increment of the heat treatment time, the reaction product layer (marked by the arrow) grows in thickness.

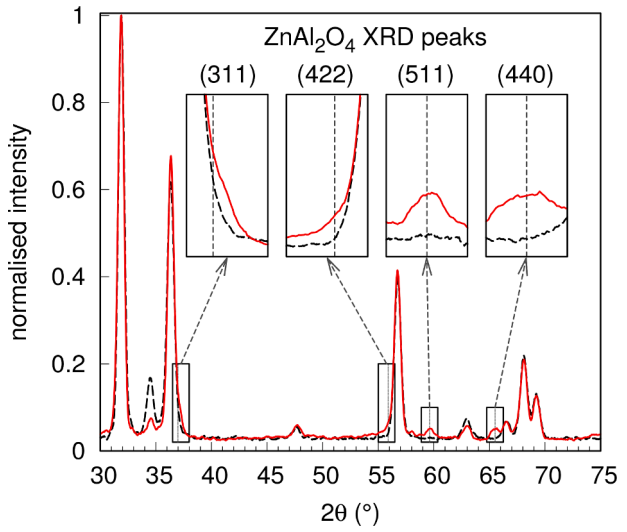

Fig. 2. GIXRD diffractograms collected after two different heat treatments. The black, dashed curve belongs to the sample after the pre-treatment step. The red, continuous curve is the diffractogram of the sample after an additional 1920 min heat treatment at 700°C. The inserts show the positions of the most intense peaks of $ZnAl_2O_4$ [36] by vertical dashed lines. (For interpretation of the references to colour in this figure legend, the reader is referred to the web version of this article.)

We can observe this in the TSEM images (see Fig. 1e and f).

On the TSEM pictures of different lamellae, image analysis was performed. We measured the apparent widths of the product islands and the average maximum thicknesses of the "pancakes" visible on the images. Their average thicknesses were calculated from uniformly spaced measurements along the full widths of the islands. We measured the average thicknesses of the continuous product layers in the later stage with the same method. The collected data are presented in Table 1. Combining the data from the table and translating it to the schematic figure of Fig. 3, a more complete picture of $ZnAl_2O_4$ spinel formation in the solid-state reaction between crystalline ZnO and amorphous Al_2O_3 can be drawn.

Looking at the data, one can see that the average observed lateral widths of the islands are growing much faster than their average maximum thicknesses. Assuming a power law growth with time, these data suggest that the exponent is 0.8 for their apparent lateral widths and 0.28 for their average maximum thicknesses. These findings are similar in nature to the theoretical predictions of a linear lateral growth and an asymptotic maximum thickness of the islands [39].

The continuous moderate increase in maximum thicknesses of the islands we observed, instead of reaching an asymptotic maximum, can be explained by the presence of grain boundaries inside the product phase. While volume diffusion might be frozen at this low temperature, grain boundaries can contribute significantly to the amount of material diffusing through the product phase, causing the deviation of the experimental results from the idealized theoretical case. This is supported by the observation of a strong effect of grain boundaries on the solid-state reaction, confirmed by earlier experiments performed be-

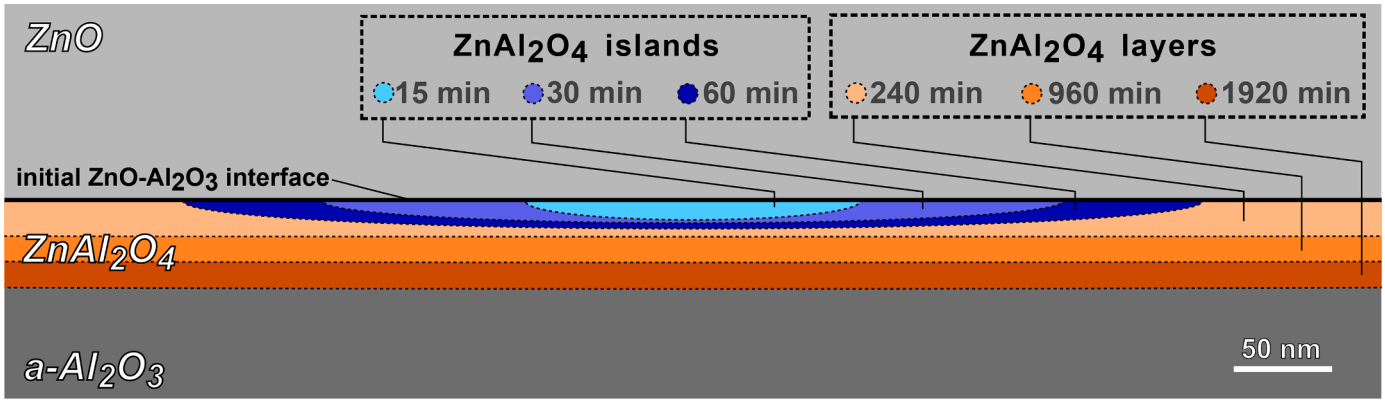

Fig. 3. Schematic figure to demonstrate the initial, two-step growth of the $ZnAl_2O_4$ spinel product phase. The continuous layer is formed by the coalescence of multiple islands. The figure is prepared to scale from the data in Table 1. The maximum thicknesses and the observed widths of the islands and also the average thicknesses of the layers are all sized to scale.

Table 1
FIB-TSEM image analysis measurement results.

Annealing time	Phase geometry	Average thickness of reaction product	Average maximum thickness of islands	Average observed width of islands
15 min	islands	7.5 nm	9.4 nm	170 nm
30 min	islands	9.0 nm	11.0 nm	376 nm
60 min	islands	9.9 nm	13.9 nm	518 nm
240 min	continuous	17.9 nm	N/A	N/A
960 min	continuous	31.0 nm	N/A	N/A
1920 min	continuous	44.4 nm	N/A	N/A

tween crystalline parent phases. In that case a significantly faster growth rate of the product phase was observed in the vicinity of the grain boundaries of the $ZnAl_2O_4$ phase (see Fig. 6. in Gorla et al. [13]).

Plotting the average thickness of the reaction product as a function of time in a double-logarithmic graph (Fig. 4), we get a 0.37 exponent value of the power law, which is significantly lower than 1.0 which was determined for the case of crystalline parent phases [13]. Furthermore, it is also lower than 0.5 what is expected for a normal, volume diffusion controlled phase growth. This is almost always an indication of a process where the main atomic transport mechanism is grain boundary diffusion through the product layer while simultaneous coarsening of the reaction product grains is taking place [57–60]. In the extreme case, when the average lateral size of the product phase grains follows a power law of $t^{0.5}$, the thickness of the product layer follows a $t^{0.25}$ power law [58].

Although the number of available data points is limited due to the difficulty of the experimental method, the deviations of the two growth stages from the function fitted to the whole growth process support the theoretical predictions. In the early stage, with product phase islands, the phase gains thickness slower (lower exponent) than during the planar growth of the later stage (higher exponent) (see Fig. 4).

Recently, Gusak [61], Gusak and Storozhuk [62] showed that assuming lateral grain growth only in the interface region can result in an increasing grain size perpendicularly to the initial interface. In this case, the thickness of the product layer follows a growth kinetics with an exponent between 0.25 and 0.5. They studied the initial condition of wide and thin, pancake-like nuclei with ca. 10 nm thickness. The analytical calculations resulted in an 0.4 growth exponent for the phase thickness, which is very close to the one we observed in our experiments. While our TSEM images are not detailed enough to prove any gradient in lateral grain size, it is evident that some type of grain coarsening is taking place in the system during phase growth. Some visible grains in Fig. 1f are clearly larger than the average island size after 15 min (see Fig. 1c).

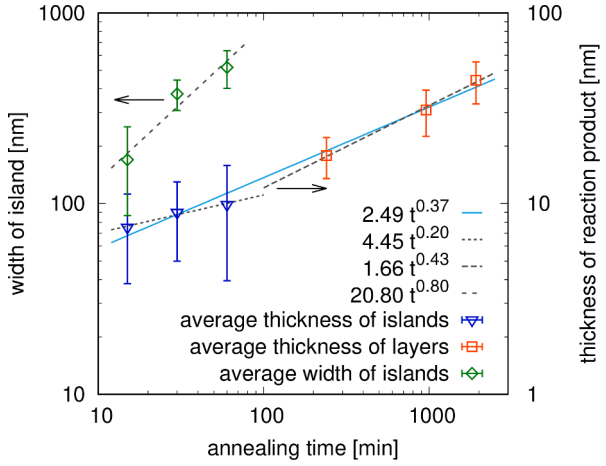

Fig. 4. Spinel island width and average thickness of the reaction product as a function of time. The thickness follows a power law with an exponent of 0.37. The exponent of the growth is lower (0.20) for the islands and higher (0.43) for the continuous layer. The average width of the islands follow a power law with an exponent of 0.80. (Note the two *y*-axes.).

In conclusion, we showed that between crystalline ZnO and amorphous Al_2O_3 a crystalline $ZnAl_2O_4$ spinel phase forms at 700°C. The reaction product grows only in the direction of the alumina phase, producing Kirkendall voids at the interface. This is an indication that the process is controlled by the diffusion of oxygen and zinc ions of ZnO. In the first stage of the solid-state reaction, the nucleation of the product phase happens in the form of flat, pancake-like islands which is followed by their fast lateral growth with negligible increase in thickness. After the formation of a continuous $ZnAl_2O_4$ layer, in the second stage of the reaction, the growth of the product phase is governed by grain boundary diffusion through the forming phase with increasing grain size. This is proven by a growth exponent of 0.37. This type of two-stage phase formation puts a lower limit on the minimum thickness of an achievable continuous product layer between the two parent phases, which can be important from an application point of view.

Declaration of Competing Interest

The authors declare that they have no known competing financial interests or personal relationships that could have appeared to influence the work reported in this paper.

Acknowledgements

Project no. TKP2021-NKTA-34 has been implemented with the support provided from the National Research, Development and Innovation Fund of Hungary, financed under the TKP2021-NKTA funding scheme. G.J. was supported by the ÚNKP-21-3-II-DE-297 New National Excellence Program of the Ministry for Innovation and Technology from the source of the National Research, Development and Innovation Fund.

Supplementary material

Supplementary material associated with this article can be found, in the online version, at doi:10.1016/j.scriptamat.2022.114857.

References

[1] Q. Zhao, Z. Yan, C. Chen, J. Chen, Chem. Rev. 117 (15) (2017) 10121–10211, https://doi.org/10.1021/ACS.CHEMREV.7B00051.
[2] Y. Okimura, H. Yokoi, K. Ohbayashi, K.-i. Shimizu, A. Satsuma, T. Hattori, Catal. Lett. 52 (1998) 157–161, https://doi.org/10.1023/A:1019060512461.
[3] X. Li, Z. Zhu, Q. Zhao, L. Wang, J. Hazard. Mater. 186 (2011) 2089–2096, https://doi.org/10.1016/j.jhazmat.2010.12.111.
[4] A. Ye, Z. Li, J. Ding, W. Xiong, W. Huang, ACS Catal. 11 (2021) 10014–10019, https://doi.org/10.1021/ACSCATAL.1C02742/SUPPL_FILE/CS1C02742_SI_001.PDF.
[5] L. Cornu, M. Gaudon, V. Jubera, J. Mater. Chem. C 1 (34) (2013) 5419–5428, https://doi.org/10.1039/C3TC30964A.
[6] S.V. Motloung, F.B. Dejene, R.E. Kroon, H.C. Swart, O.M. Ntwaeaborwa, Phys. B 468–469 (2015) 11–20, https://doi.org/10.1016/J.PHYSB.2015.04.007.
[7] P.J. Joffy, V.G. Sreeja, S. Devasia, E.I. Anila, Solid State Sci. 96 (2019) 105947, https://doi.org/10.1016/J.SOLIDSTATESCIENCES.2019.105947.
[8] G.V. Kaliyannan, S.V. Palanisamy, M. Palanisamy, M. Chinnasamy, S. Somasundaram, N. Nagarajan, R. Rathanasamy, Appl. Nanosci. (Switzerland) 9 (7) (2019) 1427–1437, https://doi.org/10.1007/S13204-018-00949-4/FIGURES/14.
[9] A. Phani, M. Passacantando, S. Santucci, Mater. Chem. Phys. 68 (2001) 66–71, https://doi.org/10.1016/S0254-0584(00)00270-4.
[10] T. Strachowski, E. Grzanka, J. Mizeracki, A. Chlanda, M. Baran, M. Małek, M. Niedziałek, Materials 15 (1) (2022), https://doi.org/10.3390/ma15010245.
[11] H.J. Fan, A. Lotnyk, R. Scholz, K.D.S. Yang, E. Pippel, S. Stephan, D. Hesse, M. Zacharias, J. Phys. Chem. C 112 (17) (2008) 6770–6774, https://doi.org/10.1021/jp712135p.
[12] Z. Li, S. Zhang, W. Lee, J. Eur. Ceram. Soc. 27 (2007) 3407–3412, https://doi.org/10.1016/j.jeurceramsoc.2007.02.195.
[13] C.R. Gorla, W.E. Mayo, S. Liang, Y. Lu, J. Appl. Phys. 87 (8) (2000) 3736–3743, https://doi.org/10.1063/1.372454.
[14] H.J. Fan, M. Knez, R. Scholz, K. Nielsch, E. Pippel, D. Hesse, M. Zacharias, U. Gösele, Nat. Mater. 5 (8) (2006) 627–631, https://doi.org/10.1038/NMAT1673.
[15] H.J. Fan, M. Knez, R. Scholz, D. Hesse, K. Nielsch, M. Zacharias, U. Gösele, Nano Lett. 7 (4) (2007) 993–997, https://doi.org/10.1021/nl070026p. PMID: 17381161.
[16] H.J. Fan, U. Gösele, M. Zacharias, Small 3 (10) (2007) 1660–1671, https://doi.org/10.1002/smll.200700382.
[17] D.S.K. Yang, M. Knez, R. Scholz, A. Berger, E. Pippel, D. Hesse, U. Gösele, M. Zacharias, J. Phys. Chem. C 112 (11) (2008) 4068–4074, https://doi.org/10.1021/jp710948j.
[18] Y. Yang, F. Güder, M. Zacharias, Isr. J. Chem. 50 (4) (2010) 439–448, https://doi.org/10.1002/ijch.201000055.
[19] Q. Peng, X.Y. Sun, J.C. Spagnola, C. Saquing, S.A. Khan, R.J. Spontak, G. N. Parsons, ACS Nano 3 (3) (2009) 546–554, https://doi.org/10.1021/NN8006543.
[20] X.Y. Chen, J.H. Li, Z.H. Sun, X. Fang, Z.P. Wei, F. Fang, X.Y. Chu, S. Li, X.H. Wang, J. Alloys Compd. 571 (2013) 114–117, https://doi.org/10.1016/j.jallcom.2013.03.198.
[21] X.Y. Chen, J.H. Li, Z.H. Sun, X. Fang, Z.P. Wei, F. Fang, X.Y. Chu, S. Li, X.H. Wang, J. Alloys Compd. 571 (2013) 114–117, https://doi.org/10.1016/J.JALLCOM.2013.03.198.
[22] E. Shkondin, H. Alimadadi, O. Takayama, F. Jensen, A.V. Lavrinenko, J. Vac. Sci. Technol. A 38 (1) (2020) 13402, https://doi.org/10.1116/1.5130176.
[23] O. Kéri, E. Kocsis, Z.K. Nagy, B. Parditka, Z. Erdélyi, Rev. Roum. Chim. 63 (5–6) (2018) 401–406.
[24] S.-Y. Pung, K.-L. Choy, X. Hou, C. Shan, Nanotechnology 19 (43) (2008) 435609, https://doi.org/10.1088/0957-4484/19/43/435609.
[25] Z. Baji, Z. Lábadi, Z.E. Horváth, G. Molnár, J. Volk, I. Bársony, P. Barna, Cryst. Growth Des. 12 (11) (2012) 5615–5620, https://doi.org/10.1021/cg301129v.
[26] C.H. Ahn, K. Senthil, H.K. Cho, S.Y. Lee, Sci. Rep. 3 (1) (2013) 2737, https://doi.org/10.1038/srep02737.
[27] J.-L. Tian, H.-Y. Zhang, G.-G. Wang, X.-Z. Wang, R. Sun, L. Jin, J.-C. Han, Superlattices Microstruct. 83 (2015) 719–729, https://doi.org/10.1016/j.spmi.2015.03.062.
[28] R. Boichot, L. Tian, M.-I. Richard, A. Crisci, A. Chaker, V. Cantelli, S. Coindeau, S. Lay, T. Ouled, C. Guichet, M.H. Chu, N. Aubert, G. Ciatto, E. Blanquet, O. Thomas, J.-L. Deschanvres, D.D. Fong, H. Renevier, Chem. Mater. 28 (2) (2016) 592–600, https://doi.org/10.1021/acs.chemmater.5b04223.
[29] S. Mishra, E. Przezdziecka, W. Wozniak, A. Adhikari, R. Jakiela, W. Paszkowicz, A. Sulich, M. Ozga, K. Kopalko, E. Guziewicz, Materials 14 (14) (2021), https://doi.org/10.3390/ma14144048.
[30] V.K. Arepalli, W.-J. Lee, Y.-D. Chung, J. Kim, Mater. Sci. Semicond. Process. 121 (2021) 105406, https://doi.org/10.1016/j.mssp.2020.105406.
[31] V. Miikkulainen, M. Leskelä, M. Ritala, R.L. Puurunen, J. Appl. Phys. 113 (2) (2013) 021301, https://doi.org/10.1063/1.4757907.
[32] M.D. Groner, F.H. Fabreguette, J.W. Elam, S.M. George, Chem. Mater. 16 (4) (2004) 639–645, https://doi.org/10.1021/cm0304546.
[33] B.L. Henke, E.M. Gullikson, J.C. Davis, At. Data Nucl. Data Tables 54 (2) (1993) 181–342, https://doi.org/10.1006/adnd.1993.1013.
[34] G. Vourlias, Coatings 10 (10) (2020), https://doi.org/10.3390/coatings10101005.
[35] V.V. Afanasev, A. Stesmans, B.J. Mrstik, C. Zhao, Appl. Phys. Lett. 81 (9) (2002) 1678–1680, https://doi.org/10.1063/1.1501163.
[36] D. Levy, A. Pavese, A. Sani, V. Pischedda, Phys. Chem. Miner. 28 (9) (2001) 612–618, https://doi.org/10.1007/s002690100194.
[37] H.J. Fan, Y. Yang, M. Zacharias, J. Mater. Chem. 19 (7) (2009) 885–900, https://doi.org/10.1039/B812619D.
[38] S. Pin, M.A. Newton, F. D'Acapito, M. Zema, S.C. Tarantino, G. Spinolo, R.A. De Souza, M. Martin, P. Ghigna, J. Phys. Chem. C 116 (1) (2012) 980–986, https://doi.org/10.1021/jp209622u.
[39] A.M. Gusak, T.V. Zaporozhets, Yu.O. Lyashenko, S.V. Kornienko, M.O. Pasichnyy, A.S. Shirinyan, Diffusion-Controlled Solid State Reactions, in: Alloys, Thin-Films, and Nano Systems, John Wiley & Sons, Ltd, 2010, https://doi.org/10.1002/9783527631025.
[40] A.M. Gusak, N.V. Storozhuk, Phys. Metals Metall. 114 (3) (2013) 197–206, https://doi.org/10.1134/S0031918X13030071.
[41] Z. Radi, P.B. Barna, J. Lábár, J. Appl. Phys. 79 (8) (1996) 4096–4100, https://doi.org/10.1063/1.361772.
[42] K.R. Coffey, L.A. Clevenger, K. Barmak, D.A. Rudman, C.V. Thompson, Appl. Phys. Lett. 55 (9) (1989) 852, https://doi.org/10.1063/1.102447.
[43] C. Michaelsen, G. Lucadamo, K. Barmak, J. Appl. Phys. 80 (12) (1996) 6689–6698, https://doi.org/10.1063/1.363794.
[44] C. Michaelsen, K. Barmak, T.P. Weihs, J. Phys. D 30 (23) (1997) 3167, https://doi.org/10.1088/0022-3727/30/23/001.
[45] G. Lucadamo, K. Barmak, D.T. Carpenter, C. Lavoie, C. Cabral, C. Michaelsen, J. M. Rickman, Mater. Res. Soc. Symp. - Proc. 562 (1999) 159–164, https://doi.org/10.1557/PROC-562-159.
[46] G. Lucadamo, K. Barmak, D.T. Carpenter, J.M. Rickman, et al., Acta Mater. 14 (49) (2001) 2813–2826. https://www.infona.pl//resource/bwmeta1.element.elsevier-36749939-58a3-3373-9877-de4b1482a4ca.
[47] G. Lucadamo, K. Barmak, K.P. Rodbell, J. Mater. Res. 16 (5) (2001) 1449–1459, https://doi.org/10.1557/JMR.2001.0202.
[48] E. Emeric, P. Gas, G. Clugnet, C. Bergman, Microelectron. Eng. 50 (1) (2000) 285–290, https://doi.org/10.1016/S0167-9317(99)00294-4.
[49] R. Delattre, O. Thomas, C. Perrin-Pellegrino, C. Rivero, R. Simola, J. Appl. Phys. 116 (24) (2014) 245301, https://doi.org/10.1063/1.4904852.
[50] M. El Kousseifi, K. Hoummada, T. Epicier, D. Mangelinck, et al., Acta Mater. 99 (2015) 1–6, https://doi.org/10.1016/j.actamat.2015.07.062.
[51] D. Mangelinck, M. El Kousseifi, K. Hoummada, F. Panciera, T. Epicier, et al., Microelectron. Eng. 199 (2018) 45–51, https://doi.org/10.1016/j.mee.2018.07.014.
[52] M. El Kousseifi, K. Hoummada, F. Panciera, C. Lavoie, D. Mangelinck, Acta Mater. 198 (2020) 100–110, https://doi.org/10.1016/j.actamat.2020.07.062.
[53] L. Klinger, Y. Bréchet, G. Purdy, Acta Mater. 46 (8) (1998) 2617–2621, https://doi.org/10.1016/S1359-6454(97)00471-0.
[54] G. Lucenko, A. Gusak, Microelectron. Eng. 70 (2–4) (2003) 529–532, https://doi.org/10.1016/S0167-9317(03)00432-5.
[55] A.M. Gusak, O.O. Bogatyrev, A.O. Kovalchuk, S.V. Kornienko, G.V. Lutsenko, Y. A. Lyashenko, A.S. Shirinyan, T.V. Zaporoghets, Usp. Fiz. Met. 5 (4) (2004) 433–502, https://doi.org/10.15407/UFM.05.04.433.
[56] M. Pasichnyy, A. Gusak. Diffusion and Diffusional Phase Transformations in Alloys, Defect and Diffusion Forum, vol. 277, Trans Tech Publications Ltd, 2008, pp. 47–52, https://doi.org/10.4028/www.scientific.net/DDF.277.47.
[57] H.H. Farrell, G.H. Gilmer, M. Suenaga, J. Appl. Phys. 45 (9) (1974) 4025–4035, https://doi.org/10.1063/1.1663907.
[58] Y.L. Corcoran, A.H. King, N. de Lanerolle, B. Kim, J. Electron. Mater. 19 (11) (1990) 1177–1183, https://doi.org/10.1007/BF02673330.
[59] A. Furuto, M. Kajihara, Mater. Trans. 49 (2) (2008) 294–303, https://doi.org/10.2320/matertrans.MRA2007192.
[60] M. Schaefer, R. Fournelle, J. Liang, J. Electron. Mater. 27 (1998) 1167–1176, https://doi.org/10.1007/s11664-998-0066-7.
[61] A.M. Gusak, Metallofiz. Noveishie Tekhnologii 42 (10) (2020) 1335–1346, https://doi.org/10.15407/MFINT.42.10.1335.
[62] A.M. Gusak, N.V. Storozhuk, Usp. Fiz. Met. 22 (4) (2021) 481–510, https://doi.org/10.15407/UFM.22.04.481.